114 *Inorg. Chem.* **2011**, *50*, 114–124
DOI: 10.1021/ic101415c

Inorganic Chemistry
Article

How Do Nitriles Compare with Isoelectronic Alkynyl Groups in the Electronic Communication between Iron Centers Bridged by Phenylenebis- and -tris(nitrile) Ligands? An Electronic and Crystal-Structure Study

Lauréline Bonniard,[†,‡] Samia Kahlal,[†,‡] Abdou K. Diallo,[§] Cátia Ornelas,[§] Thierry Roisnel,[†,‡] Gabriele Manca,[†,‡] João Rodrigues,[⊥] Jaime Ruiz,[§] Didier Astruc,*[,§] and Jean-Yves Saillard*[,†,‡]

[†]*Sciences Chimiques de Rennes, UMR CNRS No. 6226, Université de Rennes 1, 35042 Rennes Cedex, France,* [‡]*Université Européenne de Bretagne, 5 bd Laënnec, 35000 Rennes, France,* [§]*Institut des Sciences Moléculaires, UMR CNRS No. 5255, Université Bordeaux 1, 351 Cours de la Libération, 33405 Talence Cedex, France, and* [⊥]*CQM-Centro de Química da Madeira, LQCMM/MMRG, Universidade da Madeira, Campus Universitário da Penteada, 9000-390 Funchal, Portugal*

Received July 15, 2010

Density functional theory (DFT) calculations on the model $[\{FeCp(dpe)\}_2\{1,4\text{-}C_6H_4(CN)_2\}]^{2+}$ ($\mathbf{3}^{2+}$; dpe = diphosphinoethane) of salts of the cations $[\{FeCp(dppe)\}_2\{1,4\text{-}C_6H_4(CN)_2\}]^{2+}$ ($\mathbf{1}^{2+}$; dppe = 1,2-bis[diphenyldiphosphino]ethane) and $[\{FeCp^*(CO)_2\}_2\{1,4\text{-}C_6H_4(CN)_2\}]^{2+}$ ($\mathbf{2}^{2+}$), for which the X-ray crystal structures have been determined, as well as on its isomer $[\{FeCp(dpe)\}_2\{1,3\text{-}C_6H_4(CN)_2\}]^{2+}$ ($\mathbf{4}^{2+}$) and on the related complex $[\{FeCp(dpe)\}_3\{1,3,5\text{-}C_6H_3(CN)_3\}]^{3+}$ ($\mathbf{5}^{2+}$), indicate that the highest occupied molecular orbitals (HOMOs) of these compounds are localized on the metal centers with negligible participation of the C_6 ring. Thus, the poly(nitrile)phenylene ligand efficiently quenches the electronic communication between the metal centers. This is at variance with the related isoelectronic polyacetylene phenylene complexes, in which the iron centers have been shown to be electronically coupled. Consistently, apart from the case of $\mathbf{3}^{3+}$, which shows some degree of delocalization, all of the oxidized forms of $\mathbf{3}^{2+}$, $\mathbf{4}^{2+}$, and $\mathbf{5}^{2+}$ can be described as class II, localized mixed-valent species, in agreement with the electrochemical data showing two close oxidation potentials around 1 V vs $FeCp^*_2$. This is at variance with the *p*-phenylene-briged biethynyldiiron analogue, for which extended electronic delocalization was earlier shown to provide greater degree of delocalization of the mixed valency. Time-dependent DFT calculations on $\mathbf{3}^{2+}$, $\mathbf{4}^{2+}$, and $\mathbf{5}^{2+}$ indicate that the lowest-energy absorption band is associated with metal-to-ligand charge-transfer transitions involving the metallic HOMOs and the two lowest unoccupied molecular orbitals that derive from the lowest π^*(phenylene) orbitals with some π^*(CN) bonding admixture.

1. Introduction

Nitriles are good σ-donor, most often end-on two-electron ligands, although many coordination types (sometimes side-on or with various bridging types) can be found in the literature.[1] Many mononuclear transition-metal mono- and poly(nitrile) complexes are known, but acetonitrile and benzonitrile are the most well-known complexes.[1] Metal-coordinated poly(nitriles) are rarer[2] and eventually involve dendrimers.[3] Some complexes of 1,4-benzenedinitrile have also been reported by the groups of Low[4a] and Fillaut.[4b] They have also recently been used by Müller-Bauchbaum as building blocks for the construction of metal−organic frameworks.[4c]

A feature that has recently attracted the community to the nitrile complexes is the fact that nitriles are isoelectronic with acetylide anions. Acetylide complexes are being largely studied

*To whom correspondence should be addressed. E-mail: d.astruc@ism.u-bordeaux1.fr (D.A.), jean-yves.saillard@univ-rennes1.fr (J.-Y.S.).

(1) (a) Cotton, F. A.; Wilkinson, G.; Murillo, C. A.; Bochmann, M.; Storhoff, B. N.; Lewis, H. C. *Advanced Inorganic Chemistry*, 6th ed.; Wiley: New York, 1999. (b) Storhoff, B. N.; Lewis, H. C., Jr. *Coord. Chem. Rev.* **1977**, *23*, 1–29. (c) Endres, H. I. P. In *Comprehensive Coordination Chemistry*; Wilkinson, G., Gillard, J. A., Eds.; Pergamon: Oxford, U.K., 1987; Vol. *2*, p 261. (d) Michelin, R. A.; Mozzon, M.; Bertani, R. *Coord. Chem. Rev.* **1996**, *147*, 299–338.

(2) (a) Ballester, L.; Barral, M. C.; Jimenez-Aparicio, B.; Olombrada, B. *Polyhedron* **1996**, *15*, 211–217. (b) Leininger, S.; Fan, J.; Schmitz, M.; Stang, P. J. *Proc. Natl. Acad. Sci. U.S.A.* **2000**, *97*, 1380–1384. (c) Nohra, B.; Graule, S.; Lescop, C.; Réau, R. *J. Am. Chem. Soc.* **2006**, *128*, 3520–3521.

(3) (a) Newkome, G. R.; Moorefield, C. N.; Vögtle, F. *Dendrimers and Dendrons: Concepts, Syntheses, Applications*; Wiley-VCH: Weinheim, Germany, 2001. (b) Astruc, D.; Boisselier, E.; Ornelas, C. *Chem. Rev.* **2010**, *10*, 1857–1959.

(4) (a) Cordiner, R. L.; Albesa-José, D.; Roberts, R. L.; Farmer, J. D.; Puschmann, H.; Corcoran, D.; Goeta, A. E.; Howard, J. A. K.; Low, P. J. *J. Organomet. Chem.* **2005**, *690*, 4908–4819. (b) Fillaut, J.-L.; Dua, N. N.; Geneste, F.; Toupet, L.; Sinbandhit, S. *J. Organomet. Chem.* **2006**, *691*, 5610–5618. (c) Müller-Bauchbaum, K. *Inorg. Chem.* **2008**, *47*, 10141–10149.

 Published on Web 11/30/2010

for their molecular electronic properties involving mixed valency.[5] Therefore, it was of interest to investigate to what extent arene-bridged poly(nitrile) complexes could also present original electronic properties. Recently, we reported the synthesis of mono-, bis-, and trinuclear and dendritic polynuclear arenenitrileiron complexes[6] upon visible-light photolysis of the sandwich complex [FeCp(η^6-toluene)][PF_6] (Cp = η^5-cyclopentadienyl) in dichloromethane in the presence of 1,2-bis[diphenyldiphosphino]ethane (dppe).[7] All of the polynuclear iron(II) arenenitrile complexes obtained in this way showed a single oxidation wave in cyclic voltammetry, except the 1,4-benzenebis(nitrile) complex [{FeCp(dppe)}$_2${1,4-$C_6H_4(CN)_2$}][$(PF_6)_2$], for which a slight splitting of the two oxidation waves was observed ($E_{1/2}$ = 0.925 and 1.01 V vs $[FeCp^*_2]^{+/0}$),[8] indicating the existence of mixed-valence compounds under electrochemical conditions. Low's group observed a splitting of 0.07 V and concluded that the two iron centers were independent. We had not observed a wave splitting for the tris(nitrile)triiron complex [{FeCp(dppe)}$_3$-{1,3,5-$C_6H_4(CN)_3$}][$(PF_6)_3$], for which a single oxidation wave was observed at 0.98 V vs $[FeCp^*_2]^{+/0}$. This indicated that electronic communication through the *p*-bis(nitrile)-1,4-phenylene bridge is more efficient than that between the nitrile groups in the meta position relative to another, although the splitting of the waves in cyclic voltammetry does not necessarily reflect only the electronic communication between two redox centers (vide infra).[9,10] Such an electronic communication has been shown to be efficient for the isoelectronic binuclear bis(acetylide) complexes [FeCp*(dppe)]$_2$[1,4-$C_6H_4(CC)_2$] with a gap between the two successive oxidation waves that is much larger (typically 0.26 V)[5j] than that in the isoelectronic bis(nitrile) analogues. This showed the greater thermodynamic stability of the mixed-valence $Fe^{II}-Fe^{III}$ complexes in the bis(acetylide) than in the bis(nitrile) series in which the ligands are separated by the 1,4-phenylene moiety. There is also a report of the synthesis and crystal structure determination of homo- and heteronuclear bimetallic complexes [MM′-{1,3-$C_6H_4(CN)_2$}][$(PF_6)_2$], in which M and M′ are either two Ru-bis(dppe)Cl fragments or one Ru-bis(dppe)Cl fragment and one {FeCp(dppe)} metal fragment.[11] Taking into account the isoelectronic character of the nitrile and acetylide ligands, it was thus of interest to investigate the electronic reasons causing the decrease of electronic communication in the 1,4-phenylenebis(nitrile) complexes compared to the 1,4-phenylenebis(acetylide) analogues. Therefore, we have undertaken an electronic structure study of the phenylenebis(nitrile) complexes and of their mixed-valence and oxidized states. With this goal in mind, we have also determined their crystal structures because they are required for a precise knowledge of the bond parameters. These compounds are structurally closely related to the known bis(iron) 1,4-phenylenebis(nitrile) complexes[4a,6] and only differ by the nature of the counteranion, the cyclopentadienyl substituents, or the nature (carbonyls vs diphos) of the ancillary ligands.

2. Results and Discussion

A. Synthesis and Electrochemistry of the Diiron 1,4-$C_6H_4(CN)_2$ Complexes. The syntheses were carried out using classical routes in the $CpFe^{II}$(diphos)[12a] and Cp*$Fe(CO)_2$ series[12b,c] and are shown in Scheme 1 (see the Experimental Section).

These syntheses were achieved using different procedures (Scheme 1) from that previously used for the closely related complex (**1**)(**PF_6**)$_2$. The latter involved the visible-light photolysis of [FeCp(η^6-toluene)][PF_6], which is very efficient with the PF_6^- counteranion but does not work with BAr_4^- (Ar = 3,5-$(CF_3)_2C_6H_4$−) as the counteranion or C_5Me_5 ligand instead of C_5H_5. The compounds were fully characterized (see the Experimental Section) and crystallized (vide infra).

The electrochemical data were previously reported by Low's group[4a] and by our group[6] for (**1**)(**PF_6**)$_2$. Both reports involved *n*-Bu_4NPF_6 in CH_2Cl_2, are in agreement, and indicate the observation of two close oxidation waves around 0.9−1.0 V versus $FeCp^*_2$ that are separated by 70 or 76 mV. This small difference between the two oxidation potentials probably is the sign of a weak electronic communication between the two iron centers, especially because this splitting was not observed for the 1,3,5-tris(nitrile)benzene trinuclear analogue. The value of the corresponding comproportionation constant (K_c = 19) to form **1**$^+$[PF_6^-] is considerably lower than that encountered for the bis(ethynyl) analogue ($K_c = 3.5 \times 10^3$), strongly suggesting that the mixed-valence complex (**1**)(**PF_6**) is predominantly localized (class II), whereas the bis(ethynyl) analogue was earlier shown to be delocalized (class III).[5] The cyclic voltammogram of the complex (**1**)(**BAr_4**)$_2$, which contains the same cation but a different counteranion, was recorded here using *n*-Bu_4NBAr_4 as the supporting electrolyte in CH_2Cl_2 (Figure 1).

(5) (a) Ashby, G. S.; Bruce, M. I.; Tomkins, B. I.; Wallis, R. C. *Aust. J. Chem.* **1979**, *32*, 1003–1016. (b) Weyland, T.; Lapinte, C.; Frapper, G.; Calhorda, M. J.; Halet, J.-F.; Toupet, L. *Organometallics* **1997**, *16*, 2024–2031. (c) Paul, F.; Bondon, A.; da Costa, G.; Malvoti, F.; Sinbandhit, S.; Cador, O.; Costuas, K.; Toupet, L.; Boillot, M.-A. *Inorg. Chem.* **2009**, *48*, 10608–10624. (d) Paul, F.; Lapinte, C. *Coord. Chem. Rev.* **1998**, *178*−*180*, 431–509. Whittall, I. R.; McDonagh, A. M.; Humphrey, M. G. *Adv. Organomet. Chem.* **1998**, *42*, 291–362. (e) Whittall, I. R.; McDonagh, A. M.; Humphrey, M. G. *Adv. Organomet. Chem.* **1999**, *43*, 349–405. (f) Bruce, M. I.; Buntine, M. A.; Costuas, K.; Ellis, B. G.; Halet, J. F.; Low, P. J.; Skelton, B. W.; White, A. H. *J. Organomet. Chem.* **2004**, *689*, 3308–3326. (g) Paul, F.; da Costa, G.; Bondon, A.; Gauthier, N.; Sinbandhit, S.; Toupet, L.; Costuas, K.; Halet, J.-F.; Lapinte, C. *Organometallics* **2007**, *26*, 874–896. (h) Weyland, T.; Costuas, K.; Toupet, L.; Halet, J.-F.; Lapinte, C. *Organometallics* **2000**, *19*, 4228–4239. (i) Weyland, T.; Costuas, K.; Mari, A.; Halet, J.-F.; Lapinte, C. *Organometallics* **1998**, *17*, 5569–5579. (j) Le Narvor, N.; Lapinte, C. *Organometallics* **1995**, *14*, 634–639.

(6) Ornelas, C.; Ruiz, J.; Rodrigues, J.; Astruc, D. *Inorg. Chem.* **2008**, *47*, 4421–4428.

(7) (a) Catheline, D.; Astruc, D. *J. Organomet. Chem.* **1983**, *248*, C9–C12. (b) Catheline, D.; Astruc, D. *J. Organomet. Chem.* **1984**, *272*, 417–426.

(8) (a) Ruiz, J.; Astruc, D. *C. R. Acad. Sci., Ser. IIc: Chim.* **1998**, 21–27. (b) Ruiz, J.; Daniel, M.-C.; Astruc, D. *Can. J. Chem.* **2006**, *84*, 288–299. (c) Geiger, W. E. *Organometallics* **2007**, *26*, 5738–5765 (a historical and perspective account).

(9) (a) Richardson, D. E.; Taube, H. *Inorg. Chem.* **1981**, *20*, 1278–1285. (b) Richardson, D. E.; Taube, H. *J. Am. Chem. Soc.* **1983**, *105*, 40–51. (c) Sutton, J. E.; Sutton, P. M.; Taube, H. *Inorg. Chem.* **1979**, *18*, 1017–1024. (d) Astruc, D. *Electron Transfer and Radical Processes in Transition Metal Chemistry*; VCH: New York, 1995; Chapter 1, pp 30−44. (e) Astruc, D. *Acc. Chem. Res.* **1997**, *30*, 383–391. (f) Lapinte, C. *J. Organomet. Chem.* **2008**, *693*, 793–801. (g) Diallo, A. K.; Daran, J.-C.; Varret, F.; Ruiz, J.; Astruc, D. *Angew. Chem., Int. Ed.* **2009**, *48*, 3141–3145. (h) Robin, M. B.; Melvin, B.; Day, P. *Adv. Inorg. Chem. Radiochem.* **1967**, *10*, 247–422.

(10) (a) Barrière, F.; Camine, N.; Geiger, W. E. *J. Am. Chem. Soc.* **2002**, *124*, 7262–7263. (b) Barrière, F.; Geiger, W. E. *J. Am. Chem. Soc.* **2006**, *128*, 3980–3989. (c) Barrière, F.; Geiger, W. E. *Acc. Chem. Res.* **2010**, *43*, 1030–1039.

(11) Csók, Z.; Gaudum, C.; Rissanen, K.; Tuzi, A.; Rodrigues, J. *J. Organomet. Chem.* **2007**, *692*, 5263–5271.

(12) (a) Alonso, A. G.; Reventós, L. B. *J. Organomet. Chem.* **1988**, *338*, 249–254. (b) King, R. B.; Bisnette, M. B. *J. Organomet. Chem.* **1967**, *8*, 287–297. (c) Catheline, D.; Astruc, D. *Organometallics* **1984**, *3*, 1094–1100.

Scheme 1. [a]

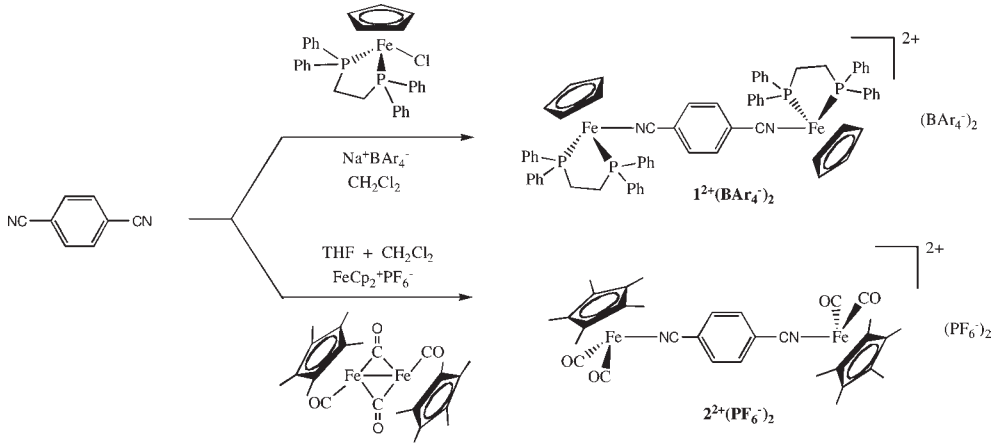

[a] Ar = 3,5-$(CF_3)_2C_6H_4$−.

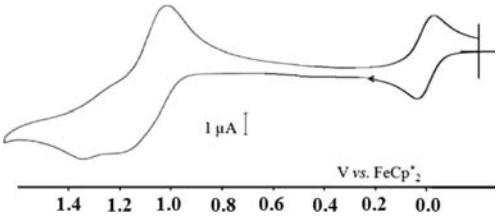

Figure 1. Cyclic voltammogram of $[\{FeCp(dppe)\}_2\{1,4\text{-}C_6H_4(CN)_2\}]^{2+}(BAr_4^-)_2]$ [**(1)(BAr$_4$)$_2$**] in CH_2Cl_2: temperature, 20 °C; supporting electrolyte, 0.1 M [*n*-Bu_4N][BAr_4]; working and counter electrodes, Pt; reference electrode, Ag; reference, $FeCp_2$* (Cp* = η^5-C_5Me_5); scan rate, 0.200 V s^{-1}. E_{p1} = 1.2 V vs $FeCp^*_2$; E_{p2} = 1.37 V vs $FeCp^*_2$.

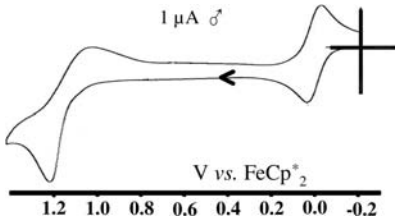

Figure 2. Cyclic voltammogram of $[\{FeCp^*(CO)_2\}_2\{1,4\text{-}C_6H_4(CN)_2\}]^{2+}(PF_6^-)_2$ [**(2)(PF$_6$)$_2$**] in CH_2Cl_2: temperature, 20 °C; supporting electrolyte, 0.1 M [*n*-Bu_4N][PF_6]; working and counter electrodes, Pt; reference electrode, Ag; internal reference, $FeCp_2$* (Cp* = η^5-C_5Me_5); scan rate, 0.200 V s^{-1}. $E_{1/2}$ = 1.075 V vs $FeCp^*_2$ (E_{pa} = 1.20 V).

It also shows two close oxidation waves at peak potentials E_{p1} = 1.2 V and E_{p2} = 1.37 V. The first one presents some chemical reversibility (with a $E_{1/2}$ value of around 1.1 V vs $FeCp^*_2$), while the second one is almost irreversible. Note that these potentials for **(1)(BAr$_4$)$_2$** are more positive than those observed for **(1)(PF$_6$)$_2$**, which is in accordance with the strong ion pairing with PF_6^- and weak ion pairing with BAr_4^-, because the positive charges are less masked in the latter than in the former. For instance, ferrocene is oxidized at a potential that is 65 mV more positive versus $FeCp^*_2$ with *n*-Bu_4NPF_6 as the supporting electrolyte than with *n*-Bu_4NBAr_4. This is due to the fact that ferricinium is sensitive to ion pairing, whereas decamethylferricinium is protected by the large ligand shells and is not significantly sensitive to counteranion effects. Not only is it more difficult to oxidize **(1)(BAr$_4$)$_2$** than **(1)(PF$_6$)$_2$**, but also the oxidized species are more destabilized than those resulting from the anodic oxidation of **(1)(PF$_6$)$_2$**, which prevents full chemical reversibility. In spite of the irreversibility of the second wave, these data are consistent with those reported earlier for **(1)(PF$_6$)$_2$** with *n*-Bu_4NPF_6 in CH_2Cl_2, confirming the weak separation between the two oxidation waves. In the case of **(2)(PF$_6$)$_2$** (Figure 2), the oxidation potentials are also more positive than 1 V (E_{pa} = 1.20 V), and the oxidation wave is also probably completely chemically irreversible, which is due to the extreme fragility of polycationic metal carbonyl complexes, especially with less than 18 valence electrons in the Fe^{III} oxidation state. At this time, no wave separation can be observed, but this has no meaning concerning the electronic structure except experimenting the evident fact that the carbonyl ligands withdraw considerable electron density from the metal compared to the diphosphine.

B. X-ray Crystal Structures of (1)(BAr$_4$)$_2$ and (2)(PF$_6$)$_2$. Figure 3 shows the X-ray structures of the $\mathbf{1}^{2+}$ and $\mathbf{2}^{2+}$ cations in compounds **(1)(BAr$_4$)$_2$** and **(2)(PF$_6$)$_2$**, respectively. Selected bond distances and angles are given in Table 1. The **(1)(BAr$_4$)$_2$** salt crystallizes in the monoclinic space group $P2_1/c$. The asymmetric unit contains one $\mathbf{1}^{2+}$ cation, which has the exact C_1 symmetry in the crystal. However, a comparison of the metrical data of the halves of the molecule indicates that it has approximate C_i symmetry, which is the highest symmetry possible for $\mathbf{1}^{2+}$, considering that the nonplanarity of the $FePC_2P$ ring forbids the existence of a mirror plane. The FeCp(dppe) units lie in a transoid conformation, with the plane containing the Cp centroids and the Fe atoms being approximately perpendicular to the central C_6 ring. The **(2)(PF$_6$)$_2$** salt crystallizes in the triclinic space group $P\bar{1}$, and the asymmetric unit contains only half of the $\mathbf{2}^{2+}$ cations, which is therefore of the exact C_i symmetry in this solid-state structure, with the $Cp^*Fe(CO)_2$ units lying in a transoid orientation. The plane containing the C_6 ring is an approximate plane of symmetry for the $Cp^*Fe(CO)_2$ units so that the molecular symmetry of $\mathbf{2}^{2+}$ is close to C_{2h}. Thus, the rotational orientations of the metallic moieties with respect to the C_6 ring in $\mathbf{1}^{2+}$ and $\mathbf{2}^{2+}$ differ by ~90°. It is likely that this rotational orientation is mainly dictated by steric and packing forces because it has been previously

Table 1. Selected Bond Distances (Å) and Angles (deg) for the $\mathbf{1}^{2+}$ (Left) and $\mathbf{2}^{2+}$ (Right) Cations in the X-ray Structures of Compounds $(\mathbf{1})(\mathbf{BAr})_2$ and $(\mathbf{2})(\mathbf{PF_6})_2$

$[\{FeCp(dppe)\}_2\{1,4\text{-}C_6H_4(CN)_2\}]^{2+}$ ($\mathbf{1}^{2+}$)		$[\{FeCp^*(CO)_2\}_2\{1,4\text{-}C_6H_4(CN)_2\}]^{2+}$ ($\mathbf{2}^{2+}$)	
Fe1−N37	1.861(3)	Fe1−N15	1.926(5)
Fe2−N87	1.867(3)		
N37−C38	1.150(5)	N15−C16	1.136(7)
N87−C88	1.143(5)		
C38−C39	1.446(6)	C16−C17	1.465(7)
C88−C89	1.440(6)		
C39−C40	1.380(6)	C17−C18	1.415(7)
C39−C41	1.394(6)	C17−C21	1.392(7)
C89−C90	1.382(6)		
C89−C91	1.392(6)		
C40−C90	1.378(5)	C18−C21	1.362(7)
C41−C91	1.381(5)		
Fe−C(Cp) (av.)	2.083(14)	Fe−C(Cp*) (av.)	2.104(11)
Fe−C(Cp) (range)	2.069(4)−2.099(5)	Fe−C(Cp*) (range)	2.089(5)−2.126(5)
Fe−P (av.)	2.197(4)	Fe1−C(O) (av.)	1.812(8)
Fe−P (range)	2.191(2)−2.201(2)	Fe−C(O) (range)	1.807(5)−1.817(6)
Fe1−N37−C38	179.4(4)	Fe1−N15−C16	176.8(5)
Fe2−N87−C88	175.7(3)		
N37−C38−C39	176.9(5)	N15−C16−C17	176.8(6)
N87−C88−C99	177.8(5)		

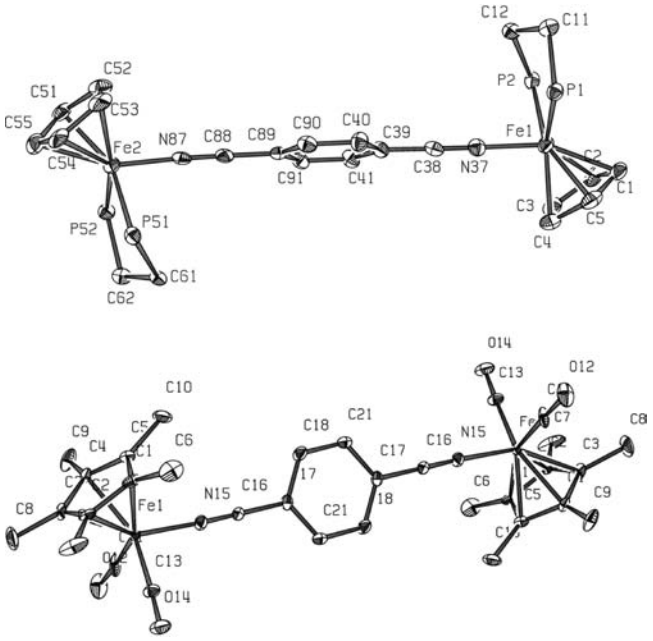

Figure 3. ORTEP views of the $\mathbf{1}^{2+}$ (top; phenyl rings omitted for clarity) and $\mathbf{2}^{2+}$ (bottom) cations in the crystal structures of $(\mathbf{1})(\mathbf{BAr})_2$ and $(\mathbf{2})(\mathbf{PF_6})_2$, respectively. Displacement ellipsoids are at the 50% and 25% probability levels, respectively.

shown by density functional theory (DFT) calculations on related isoelectronic binuclear bis(acetylide) complexes that electronic factors have negligible effects on the corresponding rotational barrier.[5b]

There are also some differences between both structures within the linker chain. The Fe−N distance is shorter in $\mathbf{1}^{2+}$ (1.864 Å in average) than in $\mathbf{2}^{2+}$ (1.926 Å). On the other hand, the N−C distance is larger (1.146 vs 1.136 Å), and the next C−C distance is shorter (1.443 vs 1.465 Å). These trends can be attributed to the fact that the $[CpFe(dppe)_2]^+$ unit is a weaker electron acceptor than $[Cp^*Fe(CO)_2]^+$. The better π-donating ability of the former tends to strengthen the Fe−N and C−C bonds and to weaken the C−N triple bond. However, these differences are not very large, and with respect to the C−N and C−C distances, they lie within (or close to) the range of experimental errors. Clearly, propagation of the metallic conjugative effect is significantly quenched by the N atoms.

C. Electronic Structure of the Diiron [1,4-$C_6H_4(CN)_2$] and [1,3-$C_6H_4(CN)_2$] Complexes. We start the analysis with the dinuclear para series $\mathbf{3}^{n+}$ (n = 2−4), in which dpe = $H_2P(CH_2)_2PH_2$ (diphosphinoethane) is taken as a simplified model for the dppe ligand in $\mathbf{1}^{n+}$. The calculations have been carried out with two different hybrid functionals, namely, B3LYP and PBE0 (see the Computational Details section). The major computed data are given in Table 2, and the structure of the dication is shown in Figure 4. Because of the nonplanarity of the coordinated dpe framework, the highest possible symmetry for a transoid conformation is C_i, and, indeed, the energy minimum of the dication was found for this symmetry group, with the same rotational orientations of the metallic moieties as those in $\mathbf{2}^{2+}$. Its optimized geometry is in good agreement with the experimental structure of the dppe relative $\mathbf{1}^{2+}$ (vide supra), except for the rotational orientation of the central C_6 ring, which differs by 90° in the two structures. This difference may originate from the different steric effects of dpe and dppe and/or the crystal packing forces in the X-ray structure of $(\mathbf{1})(\mathbf{BAr})_2$. The molecular orbital (MO) diagram of $\mathbf{3}^{2+}$ is shown in Figure 5. The large highest occupied MO (HOMO)/lowest unoccupied MO (LUMO) gap is consistent with the existence of two 18-electron iron(II) metal centers. The two lowest vacant orbitals can be identified as being the lowest π*(phenyl) orbitals, with one of them being mixed in a bonding way with π*(CN) orbitals. The six highest occupied levels are the in-phase and out-of-phase combinations of the t_{2g} orbitals of the individual metal centers. These levels have little participation on the linker. This is at variance with previous DFT results obtained on the isoelectronic model $[FeCp(PH_3)_2]_2[1,4\text{-}C_6H_4(CC)_2]$, in which the metals are linked with an all-carbon conjugated bridge.[5b,c] Obviously, the presence of a N atom on the linker largely disfavors the communication between the metals via the conjugated bridge. The weak conjugative effect between the metal centers along the linker chain is exemplified by the very small differences between the various optimized

Table 2. Major Computed Data for $[\{FeCp(dpe)\}_2\{1,4\text{-}C_6H_4(CN)_2\}]^{n+}$ ($\mathbf{3}^{n+}$; $n = 2-4$)

	$\mathbf{3}^{2+}$		$\mathbf{3}^{3+}$		$\mathbf{3}^{4+}$					
	B3LYP	PBE0	B3LYP	PBE0	B3LYP			PBE0		
	C_i, $S = 0$	C_i, $S = 0$	C_i, $S = {}^1/_2$	C_1, $S = {}^1/_2$	C_i, $S = 0$	C_i, $S = 1$	C_1, $S = BS^a$	C_i, $S = 0$	C_i, $S = 1$	C_1, $S = BS^a$
HOMO/LUMO gap (eV)	3.08	3.46			0.67			0.84		
relative energy (eV)					2.08	0.00	0.01	2.38	0.00	0.00
ionization potential (eV)			11.07	11.17	14.99	12.91	12.92	15.28	12.90	12.90
metal spin density										
Fe			0.73	1.18		1.31	−1.30		1.24	−1.34
Fe′			0.73	0.23		1.31	1.30		1.23	1.34
bond lengths (Å)										
Fe−N	1.895	1.866	1.886	1.909	1.858	2.028	2.020	1.822	1.989	1.990
Fe′−N′	1.895	1.866	1.866	1.829	1.858	2.028	2.020	1.822	1.989	1.990
N−C_1	1.169	1.166	1.176	1.170	1.118	1.167	1.167	1.179	1.164	1.164
N′−C'_1	1.169	1.166	1.176	1.172	1.118	1.167	1.167	1.179	1.164	1.164
Fe−C(Cp) (av.)	2.146	2.098	2.151	2.114	2.163	2.168	2.168	2.121	2.132	2.132
Fe′−C(Cp) (av.)	2.146	2.098	2.151	2.114	2.163	2.168	2.168	2.121	2.132	2.132
Fe−P (av.)	2.267	2.223	2.314	2.271	2.331	2.368	2.285	2.285	2.322	2.323
Fe′−P (av.)	2.267	2.223	2.314	2.271	2.331	2.368	2.285	2.285	2.322	2.323

[a] BS = broken-symmetry calculation.

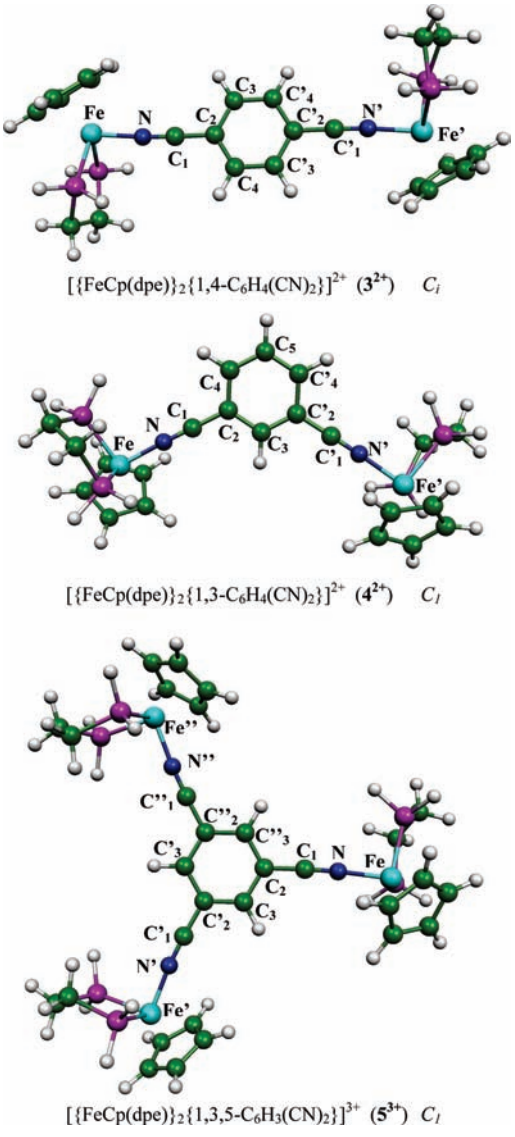

Figure 4. Optimized molecular structures of $\mathbf{3}^{2+}$, $\mathbf{4}^{2+}$, and $\mathbf{5}^{3+}$ with the atom labeling used in the tables.

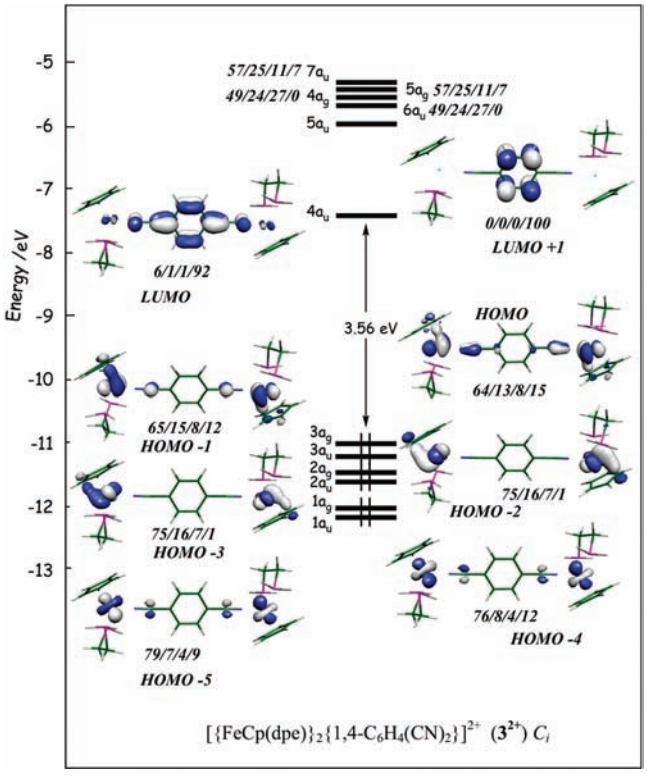

Figure 5. MO diagram of $\mathbf{3}^{2+}$ from PBE0 calculations. The fragment localization (in percent) of the MOs is given in the order $Fe_2/Cp_2/dpe_2/C_6H_4(CN)_2$.

C−N and C−C distances in $\mathbf{3}^{2+}$ and the free 1,4-$C_6H_4(CN)_2$ ligand, both at the B3LYP and PBE0 levels (largest deviation: 0.006 Å). Consistently, the energy barrier associated with a rotation of the central C_6 ring with respect to the FeCp(dpe) moieties is very low (less than 0.02 eV at both the B3LYP and PBE0 levels). Optimization of the unsaturated trication was carried out under C_1 symmetry in order to allow the metal centers to dissymmetrize, i.e., a single electron to localize on one of them. Interestingly, whereas the B3LYP calculations gave rise to a symmetrically

Table 3. Major Computed Data for $\{[Cp(dpe)Fe(NC-)]_2(1,3\text{-}C_6H_4)\}^{n+}$ ($\mathbf{4}^{n+}$; $n = 2-4$)

	$\mathbf{4}^{2+}$		$\mathbf{4}^{3+}$		$\mathbf{4}^{4+}$					
	B3LYP	PBE0	B3LYP	PBE0	B3LYP			PBE0		
	C_1, $S = 0$	C_1, $S = 0$	C_1, $S = {}^1/_2$	C_1, $S = {}^1/_2$	C_1, $S = 0$	C_1, $S = 1$	C_1, $S = BS^a$	C_1, $S = 0$	C_1, $S = 1$	C_1, $S = BS^a$
HOMO/LUMO gap (eV)	3.53	4.01			0.39			0.49		
relative energy (eV)					2.27	0.01	0.00	0.62	0.00	0.00
ionization potential (eV)			11.30	11.34	15.12	12.86	12.85	15.52	12.90	12.90
metal spin density										
Fe			1.26	1.30		1.30	−1.30		1.33	−1.33
Fe′			0.00	0.00		1.30	1.30		1.33	1.33
relative energy with respect to the 3^{n+} isomers	+0.08	+0.08	+0.31	+0.25	+0.45	+0.26	+0.24	+0.49	+0.25	+0.25
bond lengths (Å):										
Fe−N	1.901	1.871	1.982	1.952	1.905	2.025	2.020	1.867	1.982	1.982
Fe′−N′	1.901	1.871	1.878	1.851	1.905	2.025	2.020	1.867	1.982	1.982
N−C_1	1.168	1.165	1.169	1.166	1.174	1.168	1.168	1.172	1.165	1.165
N′−C'_1	1.168	1.165	1.171	1.168	1.174	1.168	1.168	1.172	1.165	1.165
Fe−C(Cp) (av.)	2.145	2.099	2.164	2.127	2.161	2.171	2.167	2.119	2.130	2.131
Fe′−C(Cp) (av.)	2.145	2.099	2.148	2.102	2.161	2.171	2.167	2.119	2.130	2.131
Fe−P (av.)	2.269	2.225	2.356	2.313	2.332	2.367	2.366	2.288	2.324	2.324
Fe′−P (av.)	2.269	2.225	2.275	2.231	2.332	2.367	2.366	2.288	2.324	2.324

[a] BS = broken-symmetry calculation.

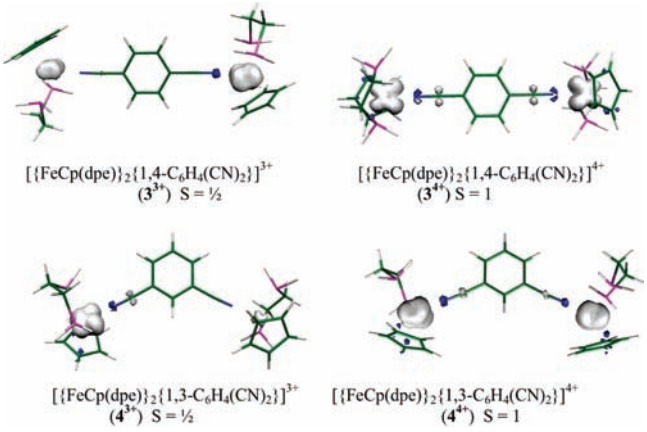

Figure 6. Plots of the spin densities computed at the PBE0 level for $\mathbf{3}^{3+}$, $\mathbf{3}^{4+}$, $\mathbf{4}^{3+}$, and $\mathbf{4}^{4+}$. The BS spin-density isocontours of $\mathbf{3}^{4+}$ and $\mathbf{4}^{4+}$ have shapes that are very similar to those of the corresponding triplet states.

optimized structure associated with an equal spin density on each metal (0.73), the PBE0 results show a localized mixed-valent species with very different iron spin densities (1.18 and 0.23), indicative of a localized Fe^{III}/Fe^{II} mixed-valence state (Table 2). A plot of the spin density computed for $\mathbf{3}^{3+}$ at the PBE0 level is shown in Figure 6. The difference in the results obtained with the PBE0 and B3LYP hybrid functionals can be rationalized by the fact that PBE0 contains more Hartree−Fock (HF) exchange contribution than B3LYP and that HF favors spin localization. Consistently, a B3LYP single-point calculation on the PBE0-optimized geometry leads to spin densities (0.90 and 0.38) that are less localized than the PBE0 ones (1.18 and 0.23). Moreover, optimization with the generalized gradient approximation (GGA)-type PBE functional (no HF contribution) leads to a fully delocalized system (iron spin densities of 0.53 and 0.53). Clearly, this monooxidized species is on the edge between localization and delocalization.

It has been shown for some mixed-valent dinuclear systems in which the metal centers are connected via an organic linker that electron delocalization can be very dependent on the rotational orientation of the linker.[13] We have tested this effect in carrying out calculations on a conformation in which the C_6 ring is rotated by 90° relatively to its ground-state orientation. Because this conformation is not stable, it was maintained during the optimization process by applying a C_s symmetry constraint, with the mirror plane bisecting the dpe ligands. This constraint forces also the dpe's to remain in the slightly less stable planar PCCP arrangement (vide supra). Under these geometrical conditions, the computed iron spin densities are 1.26 and 0.00 (B3LYP) and 1.28 and 0.00 (PBE0), i.e., consistent with a fully localized mixed-valent system. Although the spin density localization changes significantly upon rotation of the C_6 ring, the corresponding energy variation (assuming a C_s symmetry constraint) is small: 0.07 eV (B3LYP) and 0.09 eV (PBE0), in agreement with the very small contribution to the spin density of the C_6 ring: −0.003 (B3LYP) and −0.08 (PBE0) in the optimized ground state and 0.00 (B3LYP and PBE0) when the C_6 ring is rotated by 90°. These results also indicate that $\mathbf{3}^{2+}$ lies on the edge between localization and delocalization.

The dioxidized tetracationic species was calculated in its singlet and triplet states, as well as within the broken-symmetry (BS) approach. In any case, the singlet-state energy was found to be much higher (by more than 2 eV) than those corresponding to the triplet and BS calculations that are virtually equal, at both the B3LYP and PBE0 levels (Table 2). These results indicate the existence of localized single electrons. The computed spin densities (Table 2 and Figure 6) are consistent with two iron(III)

(13) (a) Benniston, A. C.; Harriman, A.; Li, P.; Sams, C. A.; Ward, M. D. *J. Am. Chem. Soc.* **2004**, *126*, 13630–13631. (b) Barybin, M. V.; Chisholm, M. H.; Dalal, N. S.; Holovics, T. H.; Patmore, N. J.; Robinson, R. E.; Zipse, D. J. *J. Am. Chem. Soc.* **2005**, *127*, 15182–15190. (c) Romańczyk, P.; Noga, K.; Wlodarczyk, A. J.; Broklawik, E. *Inorg. Chem.* **2010**, *49*, 7676–7684.

Table 4. Major Computed Data for the Cations $[\{FeCp(dpe)\}_3\{1,3,5\text{-}C_6H_3(CN)_3\}]^{n+}$ ($\mathbf{5}^{n+}$; $n = 3-5$)

	$\mathbf{5}^{3+}$		$\mathbf{5}^{4+}$		$\mathbf{5}^{5+}$					
	B3LYP	PBE0	B3LYP	PBE0	B3LYP			PBE0		
	C_1, $S = 0$	C_1, $S = 0$	C_1, $S = {}^1/_2$	C_1, $S = {}^1/_2$	C_1, $S = 0$	C_1, $S = 1$	C_1, $S = BS^a$	C_1, $S = 0$	C_1, $S = 1$	C_1, $S = BS^a$
HOMO/LUMO gap (eV)	2.96	3.43			0.33			0.42		
relative energy (eV)					1.91	0.00	0.01	2.32	0.00	0.00
ionization potential (eV)			12.74	12.80	16.16	14.24	14.25	16.64	14.32	14.32
metal spin density										
Fe			0.00	0.00		1.33	1.31		1.36	−1.36
Fe′			1.30	1.33		1.33	−1.33		1.36	1.37
Fe″			0.00	0.00		0.00	0.28		−0.28	0.14
bond lengths (Å)										
Fe−N	1.885	1.856	1.866	1.837	1.930	2.060	2.048	1.892	2.013	2.020
Fe′−N′	1.886	1.856	2.020	1.985	1.937	2.065	2.062	1.895	2.018	2.020
Fe″−N″	1.884	1.857	1.863	1.838	1.920	1.839	1.846	1.880	1.818	1.814
N−C_1	1.170	1.167	1.174	1.170	1.172	1.168	1.168	1.169	1.165	1.165
N′−C'_1	1.170	1.168	1.168	1.165	1.171	1.165	1.168	1.169	1.165	1.165
N″−C''_1	1.170	1.167	1.174	1.170	1.172	1.179	1.180	1.170	1.177	1.176
Fe−C(Cp) (av.)	2.148	2.102	2.149	2.103	2.161	2.171	2.170	2.118	2.134	2.135
Fe′−C(Cp) (av.)	2.148	2.101	2.167	2.131	2.162	2.171	2.171	2.119	2.135	2.135
Fe″−C(Cp) (av.)	2.147	2.101	2.150	2.105	2.161	2.152	2.152	2.118	2.109	2.109
Fe−P (av.)	2.273	2.229	2.283	2.239	2.325	2.372	2.367	2.280	2.330	2.330
Fe′−P (av.)	2.274	2.230	2.363	2.321	2.323	2.371	2.369	2.279	2.328	2.329
Fe″−P (av.)	2.273	2.230	2.283	2.237	2.323	2.292	2.298	2.278	2.253	2.249

[a] BS = broken-symmetry calculation.

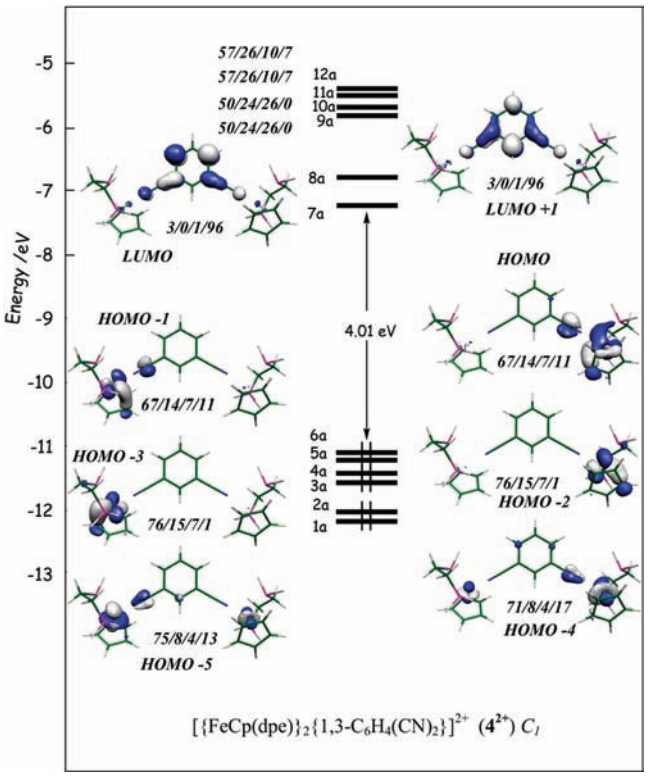

Figure 7. MO diagram of $\mathbf{4}^{2+}$ from PBE0 calculations. The fragment localization (in percent) of the MOs is given in the order $Fe_2/Cp_2/dpe_2/C_6H_4(CN)_2$.

centers. Similar calculations at the PBE level gave similar results (iron spin densities of ±1.01).

The major computed data for the dinuclear meta complexes $\{[Cp(dpe)Fe(NC-)]_2(1,3\text{-}C_6H_4)\}^{n+}$ ($\mathbf{4}^{n+}$; $n = 2-4$) are given in Table 3. It is noteworthy that each member of this meta series is found to be less stable than its homologue in the $\mathbf{3}^{n+}$ para series. The energy difference increases with the $n+$ cationic charge, whereas the corresponding free ligands are computed to be almost energy degenerate. The structure of the saturated dication is shown in Figure 2. Its energy minimum was found to have C_1 symmetry, which can be described as resulting from distortion of an ideal C_2 geometry. This distortion is caused by long-range steric repulsion between the Cp and dpe ligands so that the central $[Fe(NC-)]_2(1,3\text{-}C_6H_4)$ framework remains symmetrical. The corresponding MO diagram is depicted in Figure 7. It shows features that are very similar to those of its para relative, with even more metallic character in the two highest occupied orbitals. Contrary to its para relative, the meta trication exhibits a fully localized Fe^{III}/Fe^{II} class II mixed valence at the B3LYP level with metal spin densities of 1.26 and 0.00, respectively. A similar result is also found with the PBE0 functional (metal spin densities: 1.30 and 0.00). Rendering the two FeCp(dpe) moieties symmetry-equivalent, i.e., assuming C_2 symmetry, gives rise, of course, to a delocalized system with equal iron spin densities of 0.63 (B3LYP) and 0.65 (PBE0) and a destabilization of 0.2 eV in both cases, clearly indicating that delocalization is not favored. The results corresponding to the meta tetracation are similar to those obtained for its para relative, with a singlet state that is much higher in energy than the almost degenerate triplet and BS states and with computed spin densities consistent with two iron(III) centers (Table 3 and Figure 6).

D. Electronic Structure of the Triiron 1,3,5-$C_6H_3(CN)_3$ Series. The major computed data for the saturated trinuclear iron complex $\{[Cp(dpe)Fe(NC-)]_3(1,3,5\text{-}C_6H_3)\}^{3+}$ ($\mathbf{5}^{3+}$) are given in Table 4, and its MO diagram is depicted in Figure 8. Although the energy minimum is found to be with C_1 symmetry, the tris(nitrile)phenylene bridge is not far from D_{3h} symmetry. The computed HOMO/LUMO gap is close to the values found for $\mathbf{3}^{2+}$ and consistent with the existence of three 18-electron iron(II) centers, as well as the existence of a block of nine HOMOs made of

combinations of the t_{2g} orbitals of the three individual metal centers. As for $\mathbf{3}^{2+}$ and $\mathbf{4}^{2+}$, these levels have very little participation on the central ring (see Figure 8). On the other hand, the two LUMOs have little metal participation. They are made of the lowest π^*(phenyl) orbitals with some π^*(CN) bonding admixture. They are closely related to the two LUMOs of $\mathbf{3}^{2+}$ and (even more) of $\mathbf{4}^{2+}$, but in the case of $\mathbf{5}^{3+}$, they are close to degeneracy and isolated in the energy scale due to the pseudo-3-fold symmetry. Clearly, as in the case of $\mathbf{3}^{2+}$ and $\mathbf{4}^{2+}$, there is very little communication between the metal centers.

The monooxidized $\mathbf{5}^{4+}$ species (Table 4) exhibits a fully localized $Fe^{II}/Fe^{III}/Fe^{II}$ mixed valence, at both the B3LYP and PBE0 levels, with iron(III) spin densities of 1.30 and 1.33, respectively. Similarly to the dioxidized dinuclear species $\mathbf{3}^{4+}$ and $\mathbf{4}^{4+}$, the singlet state of $\mathbf{5}^{5+}$ is found to be much less stable than the corresponding triplet and BS states, which are almost degenerate and correspond to a localized $Fe^{III}/Fe^{III}/Fe^{II}$ mixed valence (see Figure 9),

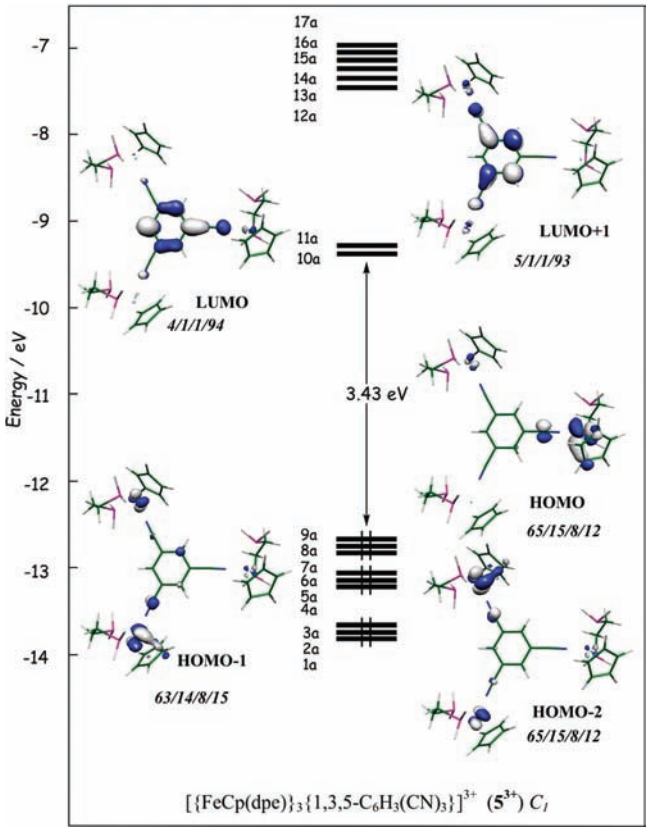

Figure 8. MO diagram of $\mathbf{5}^{2+}$ from PBE0 calculations. The fragment localization (in percent) of the MOs is given in the order $Fe_3/Cp_3/dpe_3/C_6H_3(CN)_3$.

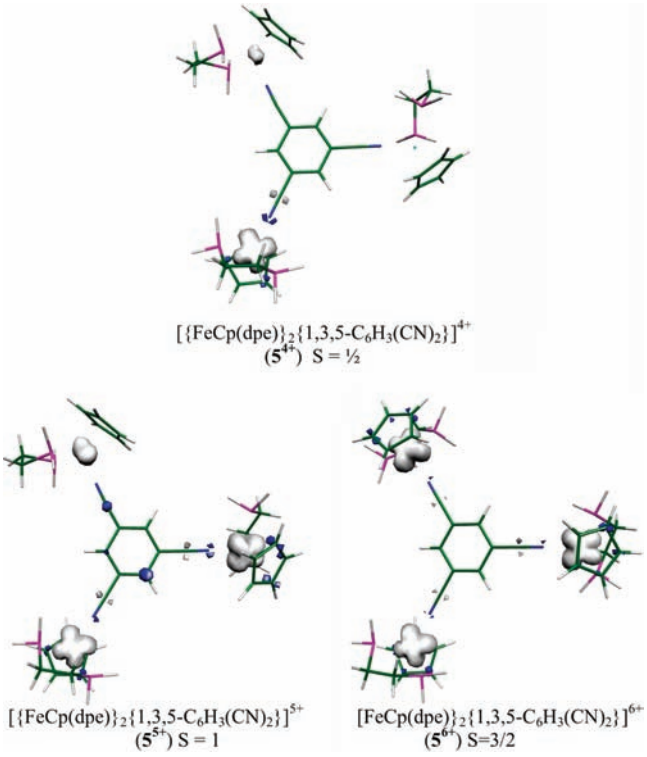

Figure 9. Plots of the spin densities computed at the PBE0 level for $\mathbf{5}^{4+}$, $\mathbf{5}^{5+}$, and $\mathbf{5}^{6+}$.

Table 5. Major Computed Data for $\mathbf{5}^{6+}$

	B3LYP			PBE0		
	C_1, $S = {}^1/_2$	C_1, $S = {}^3/_2$	C_1, S = BS[a]	C_1, $S = {}^1/_2$	C_1 $S = {}^3/_2$	C_1, S = BS[a]
relative energy (eV)	0.06	0.00	0.01	0.01	0.00	0.01
ionization potential (eV)	15.99	15.93	15.94	16.02	16.01	16.02
metal spin density						
Fe	1.39	1.36	1.39	1.42	1.42	1.42
Fe′	1.39	1.39	1.39	1.42	1.42	1.42
Fe″	−1.37	1.39	1.39	−1.41	1.42	−1.41
bond lengths (Å)						
Fe−N	2.154	2.146	2.148	2.077	2.073	2.077
Fe′−N′	2.151	2.152	2.147	2.078	2.079	2.078
Fe″−N″	2.146	2.149	2.149	2.071	2.079	2.071
N−C_1	1.167	1.169	1.167	1.164	1.164	1.164
N′−C'_1	1.167	1.167	1.167	1.164	1.164	1.164
N″−C''_1	1.167	1.167	1.167	1.164	1.164	1.164
Fe−C(Cp) (av.)	2.177	2.176	2.177	2.141	2.140	2.141
Fe′−C(Cp) (av.)	2.177	2.177	2.177	2.140	2.141	2.140
Fe″−C(Cp) (av.)	2.174	2.177	2.176	2.140	2.140	2.140
Fe−P (av.)	2.381	2.382	2.382	2.341	2.343	2.341
Fe′−P (av.)	2.380	2.381	2.382	2.341	2.341	2.341
Fe″−P (av.)	2.379	2.380	2.382	2.342	2.341	2.341

[a] BS = broken-symmetry calculation.

Table 6. Major UV−Vis Transitions ($\lambda > 250$ nm) Computed at the TDDFT Level[a]

3^{2+}			4^{2+}			5^{3+}		
wavelength (nm)	oscillator strength	transition	wavelength (nm)	oscillator strength	transition	wavelength (nm)	oscillator strength	transition
453	0.32	MLCT	394	0.11	MLCT	485	0.11	MLCT
337	0.15	MLCT	305	0.29	MLCT	477	0.10	MLCT
269	0.13	LLCT	257	0.32	LLCT	457	0.27	MLCT
						257	0.15	LLCT

[a] Only transitions with oscillator strengths larger than 0.10 are reported.

although the BS state shows some spin localization on the iron(II) center. The trioxidized species $\mathbf{5}^{6+}$ (Table 5 and Figure 9) formally corresponds to the existence of three 17-electron metal centers. It has an odd number of electrons and was computed for $S = {}^1/_2$ and ${}^3/_2$ and for the BS state. As for all of the computed dioxidized complexes, the high-spin ($S = {}^3/_2$) and BS states were found to be almost degenerate. On the other hand, in this particular case, the low-spin ($S = {}^1/_2$) state was found to lie very close to the former (0.06 eV above at the B3LYP level and almost degenerate at the PB0 level). It turns out that the $S = {}^1/_2$ and BS calculations yielded very similar results in terms of electronic structures and spin densities, especially in the case of the PBE0 calculations. As for most of the computed mixed-valent species in the title series, $\mathbf{5}^{6+}$ is found to be a fully localized $Fe^{III}/Fe^{III}/Fe^{III}$ system.

E. Electronic Absorption Spectra of the Saturated Diiron [1,4-$C_6H_4(CN)_2$] and [1,3-$C_6H_4(CN)_2$] and Triiron 1,3,5-$C_6H_3(CN)_3$ Complexes ($\mathbf{3}^{2+}$, $\mathbf{4}^{2+}$, and $\mathbf{5}^{3+}$). The UV−vis optical transitions of $\mathbf{3}^{2+}$, $\mathbf{4}^{2+}$, and $\mathbf{5}^{2+}$ have been calculated by means of time-dependent DFT (TDDFT) calculations. The computed transitions of lowest energy are given in Table 6. The corresponding simulated spectra are provided as Supporting Information (Figures S1−S3). The three simulated spectra exhibit rather similar shapes, especially those of $\mathbf{3}^{2+}$ and $\mathbf{5}^{3+}$, which exhibit a strong low-energy absorption band around 450 nm. For the three compounds, the two bands at lower energy are associated with metal-to-ligand charge-transfer (MLCT) transitions involving the highest levels of the t_{2g} blocks and the π^*(phenyl)/π^*(CN) LUMOs. The ligand-to-ligand charge-transfer (LLCT) transitions appear only at wavelengths lower that ~270 nm. Interestingly, the experimental UV−vis spectra of $[\{Cp(dppe)Fe(NC-)_2\}(1,4\text{-}C_6H_4)]^{2+}$ (related to $\mathbf{3}^{2+}$) and $[\{FeCp(dppe)\}_3\{1,3,5\text{-}C_6H_3(CN)_3\}]^{3+}$ (related to $\mathbf{5}^{3+}$) have been reported.[6] There is rather good agreement between these experimental spectra and those computed for $\mathbf{3}^{2+}$ and $\mathbf{5}^{3+}$. However, the strong low-energy absorption bands of the dppe relatives exhibit two maxima or shoulders (408/469 and 407/466 nm, respectively), whereas the simulated spectra of $\mathbf{3}^{2+}$ and $\mathbf{5}^{3+}$ show only one absorption maximum. We suggest that the lowest of the two maxima experimentally observed for the dppe relatives involves transitions from t_{2g} combinations to π^*(phenyl) orbitals of the dppe ligands. With simple dpe ligands, these transitions are missing in $\mathbf{3}^{2+}$ and $\mathbf{5}^{3+}$.

3. Concluding Remarks

It clearly appears from the above calculations that the poly(nitrile)phenylene ligand efficiently quenches the electronic communication between the iron centers to which it is bonded. Contrary to the C≡C bond, the C≡N bond has low-energy π-bonding orbitals, due to the low energy of the 2p(N) shell. As a consequence, the π-type HOMOs of the free conjugated linker have little nitrogen participation. In the complexes, this situation disfavors mixing of the linker π-type MOs with the t_{2g} metallic orbitals. A different situation occurs in the related bis(acetylide) complexes $[FeCp^*(dppe)]_2[1,4\text{-}C_6H_4(CC)_2]$,[5] because the π-bonding orbitals associated with the C≡C bonds mix to a substantial extent with both the t_{2g} and C_6 orbitals. On the other hand, the antibonding π^*(C≡N) orbitals have minor participation on nitrogen and cannot significantly mix with the t_{2g} levels. Mulliken charge analyses confirm this picture and indicate that the Fe−C bonding interaction is of the largely dominating σ-type, whatever the metal oxidation state is. Nevertheless, some π-type electronic relaxation occurs upon first oxidation in the case of the bis(nitrile) complexes. For example, when going from $\mathbf{3}^{2+}$ to $\mathbf{3}^{3+}$ and to $\mathbf{3}^{4+}$, the net charge of the phenylenebis(nitrile) linker changes from +0.39 to +0.36 and to +0.59 (PBE0 calculations); i.e., the first oxidation of $\mathbf{3}^{2+}$ tends to slightly reduce the linker. This ligand charge variation is dominated by the nitrogen charge change that varies from +0.01 to −0.07 when going from $\mathbf{3}^{2+}$ to $\mathbf{3}^{3+}$. A similar trend on the nitrogen charge is found for the related meta series, but in this case, the net charge of the whole linker changes monotonously from +0.43 to +0.48 and to +0.60 when going from $\mathbf{4}^{2+}$ to $\mathbf{4}^{3+}$ and to $\mathbf{4}^{4+}$. The particular behavior on $\mathbf{3}^{2+}$ upon first oxidation may be related to its (weak) tendency for delocalization. Thus, apart from the case of $\mathbf{3}^{3+}$, which shows some degree of delocalization, all of the oxidized forms of $\mathbf{3}^{2+}$, $\mathbf{4}^{2+}$, and $\mathbf{5}^{2+}$ can be described as localized mixed-valent class II species.[9f] The oxidation potentials of the para disubstituted phenylene complexes $[\{FeCp(dppe)\}_2\{1,4\text{-}C_6H_4(CN)_2\}][(PF_6)_2]$ [**(1)(PF$_6$)$_2$**], for which a slight splitting of the two oxidation waves has been observed previously, indicate a weak electronic communication between the two iron centers, consistent with a predominantly localized (class II) mixed-valence stabilization for **(1)(PF$_6$)**.

It is difficult to draw a simple relationship between the oxidation potentials of $\mathbf{1}^{2+}$ and $[\{FeCp(dppe)\}_3\{1,3,5\text{-}C_6H_3(CN)_3\}]^{3+}$ and the computed ionization potentials of their close relatives $\mathbf{3}^{2+}$ and $\mathbf{5}^{3+}$. It is, however, noteworthy that the difference between the computed first and second ionization potentials in the complex $\mathbf{3}^{2+}$ (1.84 eV/B3LYP and 1.73 eV/PBE0) is significantly larger than that in $\mathbf{5}^{3+}$ (1.50 eV/B3LYP and 1.52 eV/PBE0). This trend does not change when thermal and entropic corrections are considered (see the Supporting Information). This is in agreement with the fact that two one-electron oxidation waves are observed in the former case and a single two-electron wave is observed in the latter. The corresponding values for the meta complex $\mathbf{4}^{2+}$ (1.55 eV/B3LYP

Table 7. Selected Crystallographic Data for **(1)**$(BAr_4)_2$ (Left) and **(2)**$(PF_6)_2$ (Right)

empirical formula	$C_{70}H_{62}Fe_2N_2P_4(BC_{32}F_{24}H_{12})_2$	$C_{32}H_{34}Fe_2N_2O_4(PF_6)_2$
fw	2893.25	912.25
cryst syst	monoclinic	triclinic
space group	$P2_1/n$	$P\bar{1}$
a (Å)	20.718(3)	8.6029(7)
b (Å)	17.560(3)	10.9967(9)
c (Å)	35.090(5)	11.6352(10)
α (deg)	90	85.971(5)
β (deg)	100.083(6)	68.255(5)
γ (deg)	90	67.117(5)
V (Å^3)	12569(3)	938.43(14)
Z	4	1
calcd density (g cm^{-3})	1.529	1.614
abs coeff (mm^{-1})	0.405	0.957
F(000)	5832	462
cryst size (mm^3)	0.55 × 0.1 × 0.02	0.52 × 0.13 × 0.09
θ range for data collection (deg)	3.4−27.48	3.76−27.45
h_{min}, h_{max}	−26, 25	−10, 11
k_{min}, k_{max}	−22, 15	−14, 14
l_{min}, l_{max}	−45, 45	−15, 14
reflns collected/unique	94 198/27 230 [R(int) = 0.139]	9702/4210 [R(int) = 0.0246]
completeness to θ_{max}	0.945	0.981
abs correction type	multiscan	multiscan
max and min transmn	0.992, 0.789	0.918, 0.602
data/restraints/param	27 230/0/1793	4210/0/278
GOF	0.967	1.083
final R indices [$I > 2\sigma(I)$]	R1 = 0.0698, wR2 = 0.1031	R1 = 0.0561, wR2 = 0.1464
R indices (all data)	R1 = 0.2196, wR2 = 0.138	R1 = 0.0635, wR2 = 0.1532
largest diff peak and hole (e A^{-3})	0.571 and −0.59	0.501 and −0.362

and 1.56 eV/PBE0) suggest that this compound has an electrochemical behavior close to that of $\mathbf{5}^{3+}$.

In conclusion, the nitrile groups quench to a rather large extent, but not totally, the electronic interaction between the iron centers in para position and totally so in meta position.

4. Experimental Section

General Data. Acetonitrile was predried over P_2O_5 and distilled under argon immediately prior to use. Tetrahydrofuran (THF) was predried over sodium foil and distilled from sodium benzophenone anion under argon immediately prior to use. Dichloromethane was distilled from calcium hydride just before use. All manipulations were carried out using Schlenk techniques or in a nitrogen-filled Vacuum Atmospheres drylab.

^{1}H NMR spectra were recorded at 25 °C with a Bruker AC 300 (300 MHz) spectrometer. ^{13}C NMR spectra were obtained in the pulsed Fourier transform mode at 75 MHz, and ^{31}P NMR spectra were obtained in at 59.6 MHz with a Bruker AC 300 spectrometer. All chemical shifts are reported in parts per million (δ, ppm) with reference to Me_4Si (TMS).

Electrochemical measurements were recorded under a nitrogen atmosphere: solvent, dichloromethane; temperature, 20 °C; supporting electrolyte, 0.1 M [n-Bu_4N][PF_6]; working and counter electrodes, Pt; reference electrode, Ag; internal reference, $FeCp^*_2$ ($Cp^* = \eta^5$-C_5Me_5); scan rate, 0.200 V s^{-1}.

Elemental analyses were performed by the Centre of Microanalysis of the Centre National de la Recherche Scientifique (CNRS) at Solaize, France.

Synthesis of {[$C_5H_5Fe(dppe)]_2$ (1,4-dicyanobenzene)}[$BAr_4]_2$ [(1) $(BAr_4)_2$; Ar = 3,5-$(CF_3)_2C_6H_4$−]. To a solution of CpFe(dppe)Cl[2] (0.067 g, 0.14 mmol) in dichloromethane (25 mL) and in the presence of $NaBAr_4$ (0.124 g, 0.14 mmol) was added 1,4-dicyanobenzene (0.009 g, 0.07 mmol). The mixture was stirred overnight under nitrogen at ambient temperature.

The solution was filtered through Celite, and the solvent was removed under vacuum. The solid residue was washed with pentane before being crystallized in dichloromethane/pentane. Red microcrystals were recovered in 25% yield (0.0175 mmol, 0.1 g). ^{1}H NMR (300 MHz, $CDCl_3$) δ 7.71−7. (m, 64H, arom. of dppe and arom. of BAr_4), 5.95 (s, 4H, CNC_6H_4CN), 4.35 (s, 10H, C_5H_5), 2.51−2.25 (m, 8H, CH_2CH_2 of dppe). ^{13}C NMR (75 MHz, $CDCl_3$) δ 134.7−129.3 (arom. of dppe, dicyanobenzene, and BAr_4), 117.5 (CNC_6H_4), 80.3 (CH of Cp). ^{31}P NMR (59.6 MHz, $CDCl_3$) δ 96.8. Anal. Calcd for $C_{134}H_{86}B_2F_{48}Fe_2N_2P_4$: C, 55.63; H, 3.00. Found: C, 55.48; H, 2.89. IR (cm^{-1}): 2217 (ν_{CN}). Cyclic voltammetry (solvent, CH_2Cl_2; supporting electrolyte, [n-Bu_4N][BAr_4]; 293 K): two almost irreversible waves, E_{pa1} = 1.2 V vs $FeCp^*_2$; E_{pa2} = 1.37 V vs $FeCp^*_2$; E_{pc} = 1.0 V vs $FeCp^*_2$.

Synthesis of {[(η^5-C_5Me_5)$Fe(CO)_2]_2$(1,4-dicyanobenzene)]}-[$PF_6]_2$ [(2)$(PF_6)_2$]. Ferricinium hexafluorophosphate (0.698 g, 2.1 mmol) was added to a dichloromethane/THF (2:1) solution of pentamethylcyclopentadienyliron(II) dicarbonyl dimer (0.5 g, 1.05 mmol),[1] and 1,4-dicyanobenzene (0.135 g, 1.05 mmol). This solution was stirred for 24 h at room temperature under nitrogen and then filtered through Celite, and the solvent was removed under vacuum. The solid residue was washed with diethyl ether before being crystallized in dichloromethane/toluene. Orange microcrystals were recovered in 72% yield (0.756 mmol, 0.650 g). ^{1}H NMR (300 MHz, CD_2Cl_2) δ 8.02 (s, 4H, CNC_6H_4CN), 1.93 (s, 30H, CH_3 of C_5Me_5). ^{13}C NMR (75 MHz, CD_2Cl_2) δ 9.3 (CH_3 of C_5Me_5), 99.7 (Cq of C_5Me_5), 115.4 (CNC_6H_5), 131.3 (Cq of C_6H_4), 134.0 (CH of C_6H_4), 209.1 (CO). Anal. Calcd for $C_{32}H_{34}F_{12}Fe_2O_4N_2P_2$: C, 42.13; H, 3.76. Found: C, 41.74; H, 3.82. IR (cm^{-1}): 842 (ν_{PF_6}), 2012, 2059 (ν_{CO}), 2208 (ν_{CN}). Cyclic voltammetry (Figure 2; solvent, CH_2Cl_2; supporting electrolyte, [n-Bu_4N]PF_6; 293 K): one chemically and electrochemically irreversible wave, with E_p = 1.20 V vs $FeCp^*_2$. The return cathodic peak at E_{pc} = 1.0 V seen in Figure 2 probably corresponds to the reduction of the oxidatively decomposed product.

(14) Frisch, M. J. et al. *Gaussian 03, Revision B.04*; Gaussian, Inc.: Pittsburgh, PA, 2003. A full reference for Gaussian programs is provided in the Supporting Information.

(15) (a) Mielich, B.; Savin, A.; Stoll, H.; Preuss, H. *Chem. Phys. Lett.* **1989**, *157*, 200–206. (b) Lee, C.; Yang, W.; Parr, R. G. *Phys. Rev. B* **1988**, *37*, 785–789. (c) Becke, A. D. *J. Chem. Phys.* **1993**, *98*, 5648–5652.

(16) (a) Perdew, J. P.; Ernzerhof, M.; Burke, K. *J. Chem. Phys.* **1996**, *105*, 9982–9985. (b) Perdew, J. P.; Burke, K.; Ernzerhof, M. *Phys. Rev. Lett.* **1996**, *77*, 3865–3868. (c) Perdew, J. P.; Burke, K.; Ernzerhof, M. *Phys. Rev. Lett.* **1997**, *78*, 1396.

Computational Details. DFT calculations were carried out using the *Gaussian 03* package,[14] employing both the B3LYP[15] and PBE1PBE (PBE0) hybrid functionals.[16] Some test calculations have been made with the GGA-type PBE functional (see the text).[16] A standard double-ξ polarized basis set, namely, the LANL2DZ set, augmented with Ahlrichs' polarization functions on all of the atoms, was used.[17] The quality of this basis set has been tested by carrying a series single-point calculations with the larger basis set Def2-TZVP[18] on the LANL2DZ-optimized geometries $\mathbf{3}^{3+}$ and $\mathbf{3}^{4+}$ with both the B3LYP and PBE0 functionals. In any case, the computed ionization energies change by less than 0.6%, and the computed spin densities are in very good agreement with those obtained with the LANL2DZ basis set. Because the optimized B3LYP and PBE0 structures were always very similar, they were characterized as true minima on the potential energy surface by frequency calculations only at the PBE0 level. The compositions of the molecular orbitals were calculated using the AOMix program.[19] The UV−vis transitions were calculated by means of TDDFT calculations,[20] with the PBE0 functional (adiabatic excitations considered). Only spin-allowed singlet−singlet transitions have been taken into account. Moreover, only transitions with nonnegligible oscillator strengths are reported and discussed. Representations of the molecular structures, molecular orbitals, and the spin densities were done using *MOLEKEL4.3*.[21] The UV−vis spectra (Figures S1−S3 in the Supporting Information) were simulated from the computed TDDFT transitions and their oscillator strengths by using the *SWizard* program,[22] with each transition being associated with a Gaussian function of full width at half-height equal to 3000 cm^{-1}.

Crystallography. Crystallographic data of $(\mathbf{1})(\mathbf{BAr_4})_2$ and $(\mathbf{2})(\mathbf{PF_6})_2$ are given in Table 7. Both X-ray structures were obtained by the collection of intensities on an APEX II Bruker-AXS diffractometer with Mo Kα radiation (λ = 0.710 73 Å) at T = 100(2) K. The structures were solved by direct methods using the *SIR97* program[23] and then refined with full-matrix least-squares methods based on F^2 (*SHELX-97*)[24] with the aid of the *WINGX*[25] program. All non-H atoms were refined with anisotropic thermal parameters. H atoms were finally included in their calculated positions.

$(\mathbf{1})(\mathbf{BAr_4})_2$. A final refinement on F^2 with 4210 unique intensities and 278 parameters converged at $wR(F^2)$ = 0.1464 [$R(F)$ = 0.0561] for 3784 observed reflections with $I > 2\sigma(I)$.

$(\mathbf{2})(\mathbf{PF_6})_2$. A final refinement on F^2 with 27 230 unique intensities and 1793 parameters converged at $wR(F^2)$ = 0.1031 [$R(F)$ = 0.0698] for 11 462 observed reflections with $I > 2\sigma(I)$.

Acknowledgment. We are grateful to Fundação para a Ciência e a Tecnologia (FCT), Portugal (Ph.D. grant to C.O.), the Institut Universitaire de France (IUF; to D.A. and J.-Y.S.), the CNRS, the Universities of Bordeaux 1 and Rennes 1, and ANR 06-NANO-026-01 for financial support.

Supporting Information Available: Crystallographic information for $(\mathbf{1})(\mathbf{BAr_4})_2$ and $(\mathbf{2})(\mathbf{PF_6})_2$, Cartesian coordinates of the DFT-optimized compounds (Table S1), optimized bond distances and relevant energetic data (Tables S2−S5), simulated UV−vis spectra of $\mathbf{3}^{2+}$, $\mathbf{4}^{2+}$, and $\mathbf{5}^{3+}$ (Figures S1−S3), MO diagrams of oxidized species (Figures S4−S11), and ^{1}H and ^{13}C NMR spectra of $(\mathbf{1})(\mathbf{BAr_4})_2$ and $(\mathbf{2})(\mathbf{PF_6})_2$. This material is available free of charge via the Internet at http://pubs.acs.org.

(17) (a) Dunning, T. H., Jr.; Hay, P. J. In *Modern Theoretical Chemistry*; Schaefer, H. F., III, Ed.; Plenum: New York, 1976; Vol. *3*, pp 1−28. (b) Hay, P. J.; Wadt, W. R. *J. Chem. Phys.* **1985**, *82*, 270–283. (c) Wadt, W. R.; Hay, P. J. *J. Chem. Phys.* **1985**, *82*, 284–298. (d) Hay, P. J.; Wadt, W. R. *J. Chem. Phys.* **1985**, *82*, 299–310.

(18) Weigend, F.; Ahlrichs, R. *Phys. Chem. Chem. Phys.* **2005**, *7*, 3297–3305.

(19) Gorelsky, S. I. AOMix program, http://www.sg-chem.net/

(20) Burke, K.; Gross, E. K. U. A Guided Tour of Time-Dependent Density Functional Theory. In *Density Functionals: Theory and Applications*; Joubert, D., Ed.; Lecture Notes in Physics; Springer: Heidelberg, Germany, 1998; Vol. *500*.

(21) Flukiger, P.; Luthi, H. P.; Portmann, S.; Weber, J. *MOLEKEL 4.3*; Swiss Center for Scientific Computing: Manno, Switzerland, 2000; http://www.cscs.ch/

(22) Gorelsky, S. I. *SWizard program*, revision 4.5; http://www.sg-chem.net/.

(23) Altomare, A.; Burla, M. C.; Camalli, M.; Cascarano, G.; Giacovazzo, C.; Guagliardi, A.; Moliterni, A. G. G.; Polidori, G.; Spagna, R. *J. Appl. Crystallogr.* **1999**, *32*, 115–119.

(24) SHELX97—Programs for Crystal Structure Analysis (Release 97-2). Sheldrick, G. M. *Acta Crystallogr., Sect. A* **2008**, *64*, 112–122.

(25) Farrugia, L. J. *J. Appl. Crystallogr.* **1999**, *32*, 837–838.